Anomalous Hall effect and spin-orbit torques in MnGa/IrMn films: Modification from strong spin Hall effect of the antiferromagnet

K. K. Meng,[1,*] J. Miao,[1] X. G. Xu,[1] Y. Wu,[1] X. P. Zhao,[2] J. H. Zhao,[2] and Y. Jiang[1,†]

[1]*School of Materials Science and Engineering, University of Science and Technology Beijing, Beijing 100083, China*

[2]*State Key Laboratory of Superlattices and Microstructures, Institute of Semiconductors, Chinese Academy of Sciences, Beijing 100083, China*

(Received 21 July 2016; revised manuscript received 29 October 2016; published 12 December 2016)

We report systematic measurements of anomalous Hall effect (AHE) and spin-orbit torques (SOTs) in MnGa/IrMn films, in which a single $L1_0$-MnGa epitaxial layer reveals obvious orbital two-channel Kondo (2CK) effect. As increasing the thickness of the antiferromagnet IrMn, the strong spin Hall effect (SHE) has gradually suppressed the orbital 2CK effect and modified the AHE of MnGa. A scaling involving multiple competing scattering mechanisms has been used to distinguish different contributions to the modified AHE. Finally, the sizeable SOT in the MnGa/IrMn films induced by the strong SHE of IrMn have been investigated. The IrMn layer also supplies an in-plane exchange bias field and enables nearly field-free magnetization reversal.

DOI: 10.1103/PhysRevB.94.214413

I. INTRODUCTION

Spin Hall effect (SHE) that converts charge currents into spin currents in a heavy metal (HM) with strong spin-orbit coupling (SOC) has attracted much interest due to its practical use in technological applications [1–8]. When a HM comes in contact with a ferromagnet (FM), the spin currents that diffuse into the FM will modify the spin dependent transport properties such as anomalous Hall effect (AHE) [9]. On the other hand, the spin currents will also exert torque on the magnetization, which is similar to spin transfer torque [10–16]. The investigation and clarification of these intriguing issues are of fundamental importance for better understanding the underlying physics.

The AHE is the most prominent phenomenon that exists in FM, which originates from the interplay between SOC and magnetism [17]. Electrons moving through a FM will acquire a transverse velocity with opposite directions for different spin orientations due to SOC. The charge currents have usually a net polarization; therefore, this spin-dependent transverse velocity will result in a net transverse anomalous Hall voltage [18]. Despite the discovery of AHE more than a century ago, only recently a more universal microscopic description is emerging. Karplus and Luttinger have proposed that the intrinsic AHE arises from the transverse velocity of Bloch electrons induced by SOC together with interband mixing [19–24]. Both Smit and Berger suggested the extrinsic mechanisms, including skew scattering and side jump, coming from the asymmetrical scattering of conduction electrons due to SOC [25–27]. To explore and distinguish the possible mechanisms of AHE, a unified scaling describing the AHE resistivity ρ_{AH} in terms of the longitudinal resistivity ρ_{XX} has always been investigated [28–33]. Considering the essence of AHE, the modification from SHE can also be explored through clarifying $\rho_{\mathrm{AH}} \sim \rho_{\mathrm{XX}}$ relations [9].

Another spin dependent transport behavior is Kondo effect, which is a striking consequence of conduction electrons coupling with localized spin or pseudospin impurities. The orbital two-channel Kondo (2CK) effect displaying exotic non-Fermi liquid (NFL) behavior arises in the intricate scenario of two conduction electrons compensating a pseudospin 1/2 impurity of a two-level system (TLS) [34]. The orbital 2CK effect from TLSs is manifested in electrical transport by a unique temperature (T) dependence in resistivity with three distinct T regimes: a low-T upturn characterized by $\Delta\rho_{XX} \sim \ln T$ for T beyond Kondo temperature T_K, followed by NFL behavior $\Delta\rho_{XX} \sim T^{1/2}$ for $T_D < T < T_K$ and deviation from $T^{1/2}$ dependence upon further cooling [34,35]. The $T^{1/2}$ dependence is a hallmark of the NFL state in the orbital 2CK effect, in striking contrast to the T^2 scaling of Fermi-liquid behavior in fully screened Kondo effect. In a conventional FM, although the Kondo coupling between the TLS and itinerant electrons is irrelevant to the electron spins, the symmetry of the two spin channels is broken due to ferromagnetic exchange splitting of the d band. The channel asymmetry should lead to different tunneling rates of a TLS for the two spin channels and thus weaken the NFL behavior. If the channel asymmetry is large enough, it should be manifested as a decreased magnitude and an enhanced effective breakdown temperature of the 2CK effect as a result of the enhanced decoupling of TLS from one spin channel [34]. Therefore, the orbital 2CK effect in the FM will be suppressed when contacting with a strong SOC metal since the pure spin current generated by SHE will diffuse into the FM layer and enhance the channel asymmetry.

Moreover, in HM/FM heterostructures with perpendicular magnetic anisotropy (PMA), the generated pure spin current can also exert torques on the magnetization, which are referred to as spin-orbit torques (SOTs) [19–24]. On the other hand, spin accumulation can take place at the FM/HM interface via the Rashba effect, which has also generated significant effective torques and caused current-induced domain nucleation and fast domain wall motion. In most previous experiments on SOT, an extra in-plane magnetic field is indeed required to achieve deterministic switching, and this is detrimental for device applications. More recently, however, the experimental demonstrations of strong SOC in antiferromagnets (AFMs) provide an alternative to HMs in HM/FM heterostructures for devices with active SOT [13,36,37]. By replacing HMs with AFMs, the purely electrical deterministic switching of

*Author to whom correspondence should be addressed: kkmeng@ustb.edu.cn

†Author to whom correspondence should be addressed: yjiang@ustb.edu.cn

perpendicular magnetization without any assistance from an external magnetic field will be realized since an AFM can supply an exchange bias field that can serve as an effective magnetic field.

In this context, as an attempt to offer a step towards exploring these rich and underlying physics, we have systematically investigated the AHE and SOT in MnGa/IrMn films, in which a single $L1_0$-MnGa epitaxial layer reveals obvious orbital 2CK effect. The strong SHE of the AFM IrMn has suppressed the orbital 2CK effect and modified the AHE of MnGa. The results are compared with MnGa/Al and MnGa/Pt films. A scaling involving multiple competing scattering mechanisms has been used to distinguish different contributions to the modified AHE. It is found that the spin-dependent transport properties in MnGa/HM (IrMn or Pt) are much different from that in the MnGa single layer and the MnGa/Al films, in which Al displays weak SHE. On the other hand, the sizeable SOT in the MnGa/IrMn films induced by the strong SHE of IrMn has also been observed. The IrMn layer supplies an in-plane exchange bias field and enables nearly field-free magnetization reversal. By performing adiabatic harmonic Hall voltage measurements, we have also quantitatively investigated the SHE induced effective field.

II. EXPERIMENTAL DETAILS

A 3-nm-thick $L1_0$-MnGa single-crystalline film was grown on a semi-insulating GaAs (001) substrate by molecular-beam epitaxy at substrate temperature $T_S = 250\,^{\circ}$C. Here, the Mn/Ga atom ratio is 1 [38]. Then, IrMn films with different thickness were immediately deposited on it by direct current (dc) magnetron sputtering. Finally, a 1.5-nm-thick Pt layer was deposited for preventing oxidation. After deposition, to provide the exchange bias, the samples were annealed at 250 °C for 30 minutes under an in-plane magnetic field of 5 KOe along the $+X$ direction. In the experiments, the 6-nm-thick Al and Pt were also deposited on MnGa for contrast experiments. Photolithography and Ar ion milling were used to pattern Hall bars, and a lift-off process was used to form the contact electrodes. A scanning electron microscope (SEM) image of a patterned Hall bar and the schematic of the measurement setup along with the definition of the coordinate system used in this study are shown in Fig. 1(a). The size of all the Hall bars is 10 μm × 80 μm. Two electrodes for current injection are labeled I_+ and I_-−. Another two electrodes for the Hall voltage measurements are labelled V_+ and V_-−. We measured the SOT induced magnetization switching by applying a pulsed current with the width 50 μs, and the resistance was measured after a 16 μs delay under an external magnetic field H_X along either positive or negative X directions. We apply a sinusoidal alternating current (ac) with the frequency of 259.68 Hz to exert periodic SOT on the magnetization. The first V_ω and the second $V_{2\omega}$ harmonic anomalous Hall voltages were measured as a function of the magnetic field H at the same time using two lock-in amplifier systems.

III. RESULTS AND DISCUSSION

The saturated magnetization $M_S$of MnGa is 170 emu/cc, which is much smaller than the theoretical value for the fully ordered $L1_0$-MnGa probably due to the loss of the chemical ordering. The effective anisotropy field H_K is given by $H_K = H_{sat} + 4\pi M_S$, where H_{sat} is the hard-axis saturation field. For MnGa/IrMn (t), H_K is calculated to be about 1.3 T, 1.1 T, and 0.8 T, respectively, as increasing t from 4 to 8 nm. The normalized anomalous Hall resistance R_{AH} versus the perpendicular magnetic field for MnGa/IrMn ($t = 0,4,6,8$ nm) were measured with applying a dc current of 1 mA, as shown in Fig. 1(b). It was obtained by subtracting the ordinary Hall component determined from a linear fit to the high-field region up to ±6 T. As t increases, the squareness of the loop decreases due to the increasing magnetic coupling between MnGa and IrMn. The inset figure shows the AHE resistivity ρ_{AH}, which decreases as increasing t from 4 to 8 nm. We have also measured the temperature dependent resistivities of single Pt, Al, and IrMn films. Then, assuming that each film in the MnGa/Pt, MnGa/Al, and MnGa/IrMn bilayers acts as a parallel resistance path, both the AHE resistivity ρ_{AH} and the longitudinal resistivity ρ_{XX} in this paper have been expressed as those of the MnGa layer.

Figures 2(a) and 2(b) plot the T dependence of the resistivity variation at $H = 0$ Oe for the $L1_0$-MnGa film, which shows distinct signatures associated with the TLS-induced 2CK effect. The longitudinal resistivity ρ_{XX} firstly varies linearly with ln$T$ as increasing T from 300 K. Then, ρ_{XX} deviates from the ln T dependence and crossover to a $T^{1/2}$ dependence when

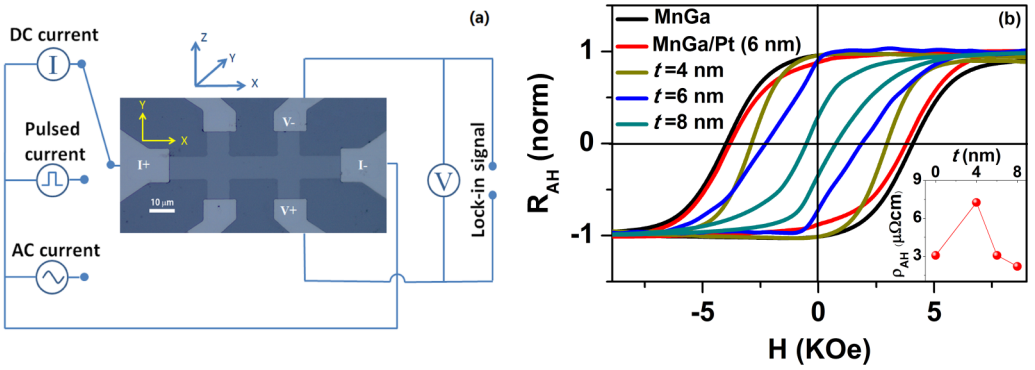

FIG. 1. (a) The SEM image of a patterned Hall bar and the schematic measurement setup along with the definition of the coordinate system. (b) Out-of-plane hysteresis loop of the normalized anomalous Hall resistance in MnGa/IrMn (t nm) and MnGa/Pt (6 nm). The inset shows the AHE resistivity ρ_{AH}.

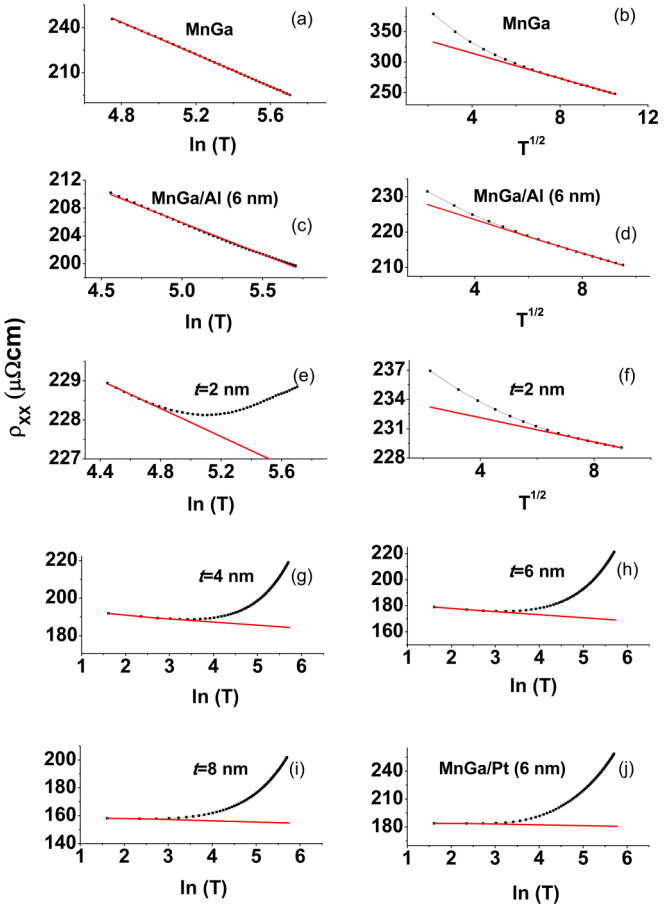

FIG. 2. The temperature dependence of the longitudinal resistivity ρ_{XX} for all the samples.

T drops below $T_K = 115$ K. The large T_K of the $L1_0$-MnGa film suggests a strong Kondo coupling between the TLS and conduction electrons. The $T^{1/2}-$ dependent resistivity is regarded as a unique signature of the NFL behavior for the 2CK effect. As further decreasing temperature, ρ_{XX} begins to increase faster than $T^{1/2}$ below a characteristic temperature $T_D = 45$ K, indicating the deviation from the NFL behavior. This represents an observation of the TLS theory-expected deviation from the orbital 2CK state below T_D in a diffusive conductor. After depositing a 6-nm-thick Al film, the orbital 2CK effect has not been changed evidently, as shown in Figs. 2(a) and 2(b). Notably, comparing the T dependence of ρ_{XX} in MnGa and MnGa/Al, evident suppression has been found in MnGa/IrMn (2 nm), as shown in Figs. 1(d) and 1(e). The ρ_{XX} for the MnGa/IrMn (2 nm) bilayer shows a resistivity

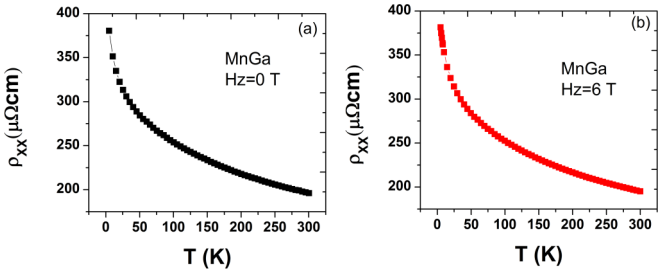

FIG. 3. The ρ_{XX} versus T at $H_Z = 0$ T (a) and $H_Z = 6$ T (b) for the $L1_0$-MnGa single layer.

minimum at a characteristic temperature ($T_M = 165$ K). In the high T regime ($T > T_M$), ρ_{XX}, increases linearly with T due to the increasing phonon scattering, and T_K decreases to 85 K. The suppression gradually increased as increasing the thickness of IrMn with further decreasing T_K and T_D, as shown in Figs. 2(g)–2(i). The 6-nm-thick Pt layer has also suppressed the orbital 2CK effect similar with MnGa/IrMn (8 nm), as shown in Fig. 2(j). The values of T_K and T_D have been summarized in Table I. In a conventional FM, although the Kondo coupling between the TLS and itinerant electrons is irrelevant to the electron spins, the symmetry of the two spin channels is broken due to ferromagnetic exchange splitting of the d band. The channel asymmetry should lead to different tunneling rates of the TLS for two spin channels and thus weaken the NFL behaviors in comparison with its nonmagnetic counterpart ($\Delta N = N_\uparrow - N_\downarrow = 0$), where $N_\uparrow$ and $N_\downarrow$ are the density of states for majority and minority spin channels in the conduction band. Based on the Stoner model for itinerant ferromagnetism, M_S can be used as an index for the degree of spin population imbalance of the conduction band. The small M_S of the MnGa film studied here indicates a very low degree of spin population imbalance with the loss of the chemical ordering. This could be the reason that the ferromagnetic exchange splitting does not quench the 2CK physics. Considering that the enhanced channel asymmetry will weaken the NFL behavior, we suppose that the orbital 2CK effect will be suppressed if the pure spin current generated by the metals with strong SOC, such as Pt or IrMn, diffuses into the FM. The Fermi surface will be modified, and the enhanced ΔN will quench the orbital 2CK effect. To establish more rigorously the orbital 2CK effect in our $L1_0$-MnGa films, we have examined the effect of the applied perpendicular magnetic fields, H_Z, on the T-dependent resistivity, as shown in Fig. 3. The H-independent resistivity upturn scaling with $\ln T$ and $T^{1/2}$ in the two T regimes and the deviation from the NFL behavior at the lowest temperatures are consistent with the TLS model.

TABLE I. T_D,T_K, the AHE scaling coefficients, and current-induced effective field H_D for the six samples.

	T_D (K)	T_K (K)	α	$\beta_0(\mu\Omega^{-1}\text{cm}^{-1})$	γ $(\mu\Omega^{-1}\text{cm}^{-1})$	$\beta_1(\mu\Omega^{-1}\text{cm}^{-1})$	H_D (Oe per 10^6 A/cm^2)
MnGa	45	115	−1.039	−4.1e-4	4.38e-4	−2.1e-4	0
MnGa/Al(6)	45	100	−1.042	−1.4e-3	6.4e-4	−7.2e-3	0
MnGa/Pt(6)	45	85	0.249	1.2e-3	−2.8e-4	1.1e-3	12
$t = 4$ nm	∼	5	0.676	7.7e-3	−4.3e-4	7.6e-3	27
$t = 6$ nm	∼	5	0.524	1.4e-3	−7.4e-4	1.4e-4	28
$t = 8$ nm	∼	5	0.569	2.1e-3	−1.5e-4	2.2e-3	31

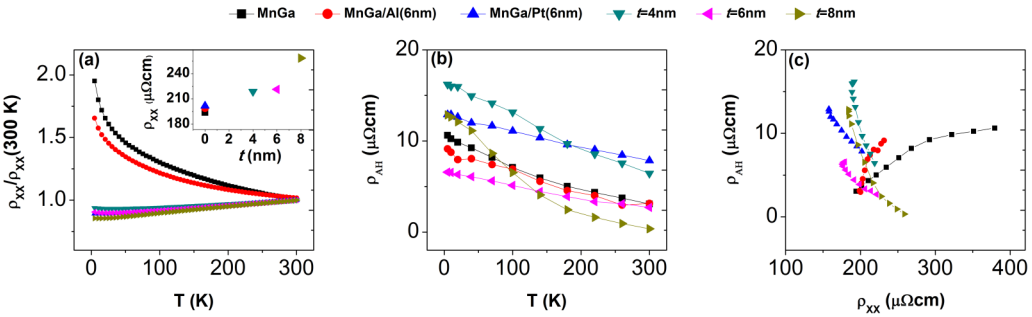

FIG. 4. (a) The temperature dependence of the longitudinal resistivity ρ_{XX} for the six samples. The data are normalized by the values at 300 K. The inset shows ρ_{XX} measured at 300 K. (b) The temperature dependence of $\rho_{\rm AH}$ for the six samples. (c) The $\rho_{\rm AH}$ as the function of ρ_{XX} for the six samples.

For clarity, we normalize the resistivity of all the samples by the value at 300 K and plot the temperature dependence of $\rho_{XX}(T)/\rho_{XX}$ (300 K) in Fig. 4(a), and the inset figure shows the ρ_{XX} for all the six films. Figure 4(b) shows the T profiles of $\rho_{\rm AH}$ for all the six samples, which all decrease as cooling down. So far, there have been few reports on a similar anomaly in the T dependence of $\rho_{\rm AH}$ [39]. We infer that the strong orbital 2CK effect in $L1_0$-MnGa could be the reason for such a complex T dependence of $\rho_{\rm AH}$. We plot $\rho_{\rm AH}$ as a function of ρ_{XX} for all the samples to compare the difference of scaling curves in Fig. 4(c). Most recently, Hou *et al.* have derived a general scaling form of the anomalous Hall resistivity as a function of multiple scattering mechanisms using [31]:

$$\rho_{\rm AH} = \alpha\rho_{xx0} + \beta_0\rho_{xx0}^2 + \gamma\rho_{xx0}\rho_{xxT} + \beta_1{\rho^2}_{xxT}, \quad (1)$$

where ρ_{XX_0} is the residual resistivity induced by impurity scattering, $\rho_{xxT} = \rho_{XX} - \rho_{XX_0}$ is due to dynamic disorders (mainly phonons at higher temperatures), α is the skew scattering coefficient, and the coefficients β_0, β_1, and γ contain intrinsic Berry curvature and side-jump contributions. Here, ρ_{XX_0} is considered as the minimum resistivity. As shown in Fig. 5, the new scaling works well for all samples except for $t = 4$ and 6 nm at low temperatures, where the orbital

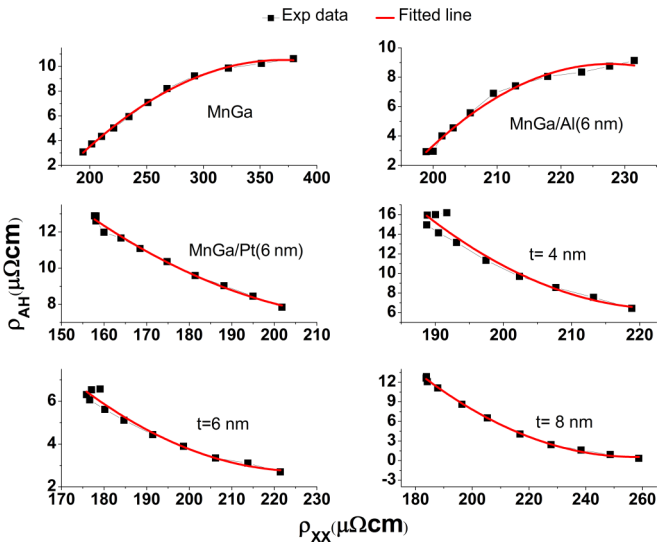

FIG. 5. The $\rho_{\rm AH}$ versus ρ_{XX} for the six samples. Black squares are experimental raw data. The red lines are fitted plots using Eq. (1).

2CK effect becomes important. The coefficients α, β_0, γ, and β_1 determined from Eq. (2) for all the samples are shown in Table I. The α is large negative in both MnGa and MnGa/Al (6 nm), which should be due to the extrinsic AHE contribution from impurities and static defects with the loss of chemical ordering. However, it changes into relatively small positive in MnGa/Pt (6 nm) and MnGa/IrMn (t). Considering that the chemical ordering of MnGa has not been changed, the variation of skew scattering should partly come from the asymmetric scattering due to the effective SOC at the interface and partly come from the modification of the Fermi surface with injected spin-polarized current. On the other hand, as discussed by Hou *et al.*, it seems challenging to separate out the intrinsic part from the side-jump one in β_0, β_1, and γ [31]. However, $(\beta_0 + \beta_1 - \gamma)$ and $(\gamma - 2\beta_1)$ are the coefficients of pure scattering effect, and they have also changed sign with contacting HMs. Totally speaking, the contacting HMs have introduced spin-dependent scattering at interface due to SOC and spin polarized current, which modified the Fermi surface of MnGa.

To further verify the modification from SHE, we have carried out SOT measurements for MnGa/IrMn ($t = 4,6,8$ nm) and MnGa/Pt (6 nm) at room temperature. The current-induced magnetization switching with applying an in-plane field of H_X is shown in Fig. 6. For MnGa/IrMn (4 nm), the magnetization is switched from $+Z$ to $-Z$ with $H_X = +3$ KOe when sweeping the current from positive to negative and is switched back from $-Z$ to $+Z$ when sweeping the current reversely. With $H_X = -3$ KOe, the opposite switching behavior is observed. The switching current density is about 1.5×10^8 A/cm^2. As decreasing the absolute value of H_X, the magnetization could not be fully switched, and no switching at $H_X = 0$ Oe occurs. Therefore, the SHE of IrMn exerts torques on the magnetization of MnGa, but nearly no exchange bias field exists. It also indicates that the IrMn has a positive spin Hall angle, which is consistent with a previous study on the inverse SHE in IrMn [40,41]. As increasing t to 6 nm, the switching behavior at the positive and negative applied field is not symmetric. Partial magnetization has been switched at 0 Oe, indicating that a weak exchange bias field has been induced in the films. This phenomenon becomes more evident in MnGa/IrMn (8 nm), in which a nearly field-free switching has been observed. The magnetic properties of MnGa have been influenced by the IrMn layer along perpendicular axes, which becomes more evident with increasing t. First, as shown in Fig. 1(b), as increasing the thickness of IrMn to 8 nm, the

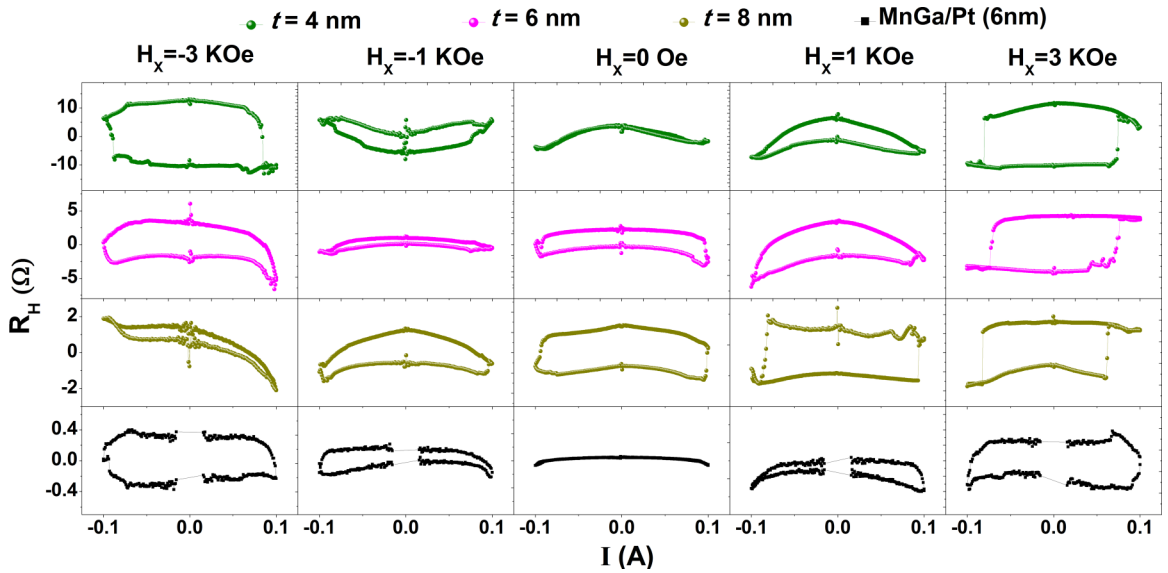

FIG. 6. R_H-I curves in MnGa/IrMn ($t = 4,6,8$ nm) and MnGa/Pt (6 nm) under different in-plane external fields H_X.

coercivity of the bilayers has been decreased from 5 KOe to 1 KOe. On the other hand, according to the SOT results, the exchange bias effect also happened along the X axis, and the exchange bias field is about $2 \sim 3$ KOe. The AFM IrMn has not only generated SOT but also supplied an in-plane exchange bias field, which enables all-electrical deterministic switching of perpendicular magnetization in the absence of magnetic field. However, for MnGa/Pt (6 nm), it is found that the magnetization of MnGa cannot be fully switched, mostly because the spin Hall angle of Pt is smaller than IrMn and the SHE is weak.

To determine the strength of spin-orbit effective fields in the MnGa/IrMn films, we have performed nonresonant magnetization-tilting measurements by applying a small amplitude low frequency ac with the amplitude of 2.1 mA through the device and simultaneously sweeping a static in-plane magnetic field parallel or perpendicular to the current direction (H_X and H_Y). The dampinglike H_D and fieldlike effective fields H_F can be calculated by [6]

$$H_{D(F)} = -2\frac{\partial V_{2\omega}/\partial H_{X(Y)}}{\partial^2 V_\omega/\partial H_{X(Y)}^2}. \tag{2}$$

Figure 7 shows the first harmonic V_ω and second harmonic Hall voltages $V_{2\omega}$ plotted against the in-plane external field H_X, which are measured with out-of-plane magnetization component $M_Z > 0$ and with $M_Z < 0$. Before the harmonic measurement shown in Fig. 7, we have applied a large out-of-plane external field to saturate the films of $t = 4$ nm, $t = 6$ nm, and MnGa/Pt (6 nm), which remain saturated after the field is turned off. The remanence is small for the film of $t = 8$ nm, as shown in Fig. 1(b); however, the method mentioned above is based on the assumption of a uniformly magnetized PMA film with the magnetization tilted from the perpendicular axis at a small angle. Therefore, we have first applied a large out-of-plane external field to saturate the film and carried out

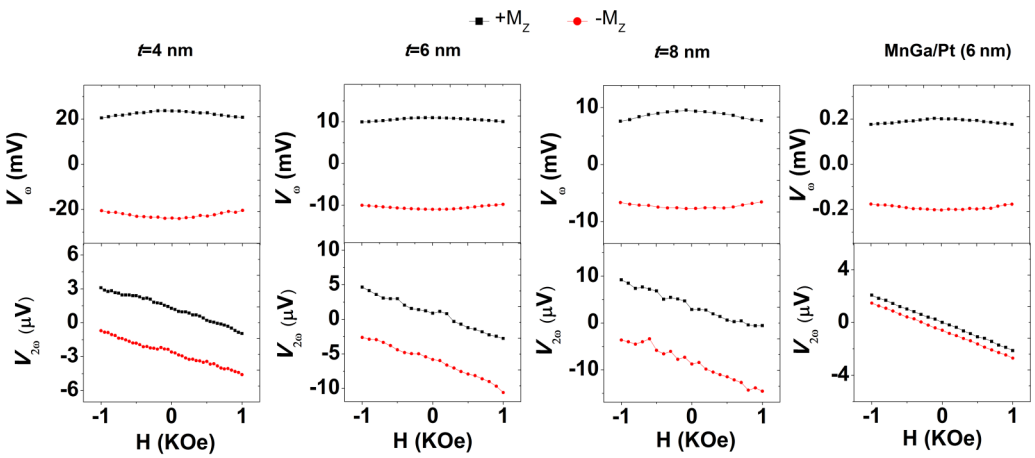

FIG. 7. The first V_ω and second $V_{2\omega}$ harmonic Hall voltages plotted against the in-plane external fields H_X for the four samples.

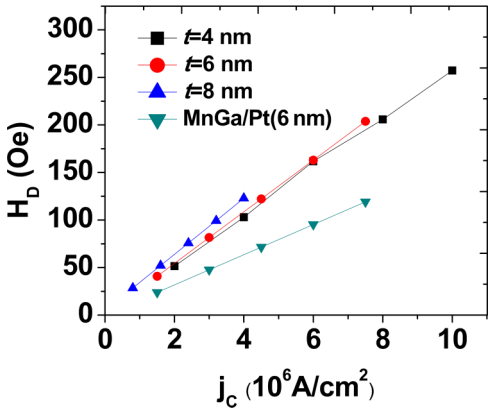

FIG. 8. Current-induced effective field H_D versus applied ac current density for the four samples.

the second harmonic measurement for the $t = 8$ nm film with switching H_X and keeping H_Z at ± 800 Oe to realize more out-of-plane magnetization and to better signal to noise. On the other hand, there is no obvious $V_{2\omega}$ signal with H_Y applied, indicating that the fieldlike SOT is largely eliminated in the films. We have also extracted the effective spin Hall angle $\theta_{SH} = 0.27$ of IrMn in MnGa/IrMn and $\theta_{SH} = 0.11$ of Pt in MnGa/Pt using the relation $H_D = \hbar\theta_{SH}|J_C|/(2|e|M_S t_F)$, where J_C is charge current density, e is the charge of an electron, M_S is the saturation magnetization of MnGa, and t_F is the thickness of the MnGa [42]. The value of IrMn is larger than the result in the previous studies [41], which may be ascribed to the different experimental method. Figure 8(a) shows the estimated H_D with out-of-plane magnetization component $M_Z < 0$ using Eq. (2) as applied current density J_C. The magnitude of H_D increases to be 31 Oe per 10^6 A/cm^2 as t increases to be 8 nm.

On the other hand, anomalous Nernst effect (ANE) may also contribute to the second harmonic voltage. We have carried out the harmonic measurement with sweeping the magnetic field along X direction to detect the ANE due to vertical thermal gradient, as shown in Fig. 9. As discussed in the work of Avci *et al.* [43], the SOT contribution tends to vanish as the external field is large enough to force the magnetization to align rigidly along the field direction. The ANE, on the other hand, depends only on the magnetization direction and should be independent of the external field amplitude (provided that the magnetization is saturated). It is found that in the MnGa/Pt (6 nm) film, the second harmonic signal becomes very small as the field is large enough, indicating that it comes from the SOT effect and ANE is small. However, the hysteresis behaviors have been observed in all of the MnGa/IrMn (t) films. Though the magnetization is saturated, as shown in the first harmonic signals, the second harmonic signals for the $t = 4$ and 6 nm films become larger, which cannot be ascribed to SOT or ANE. In this case, the complex domain structure of the MnGa/IrMn films may play a dominant role since IrMn not only provides a spin-polarized current due to SHE but also is an AFM. For the $t = 8$ nm film, the second harmonic signal becomes constant under larger fields, which is ascribed to the hybrid effect of SOT, ANE, and a complex domain structure. On the other hand, a shift has been found in the first harmonic curve in $t = 8$ nm film, as shown in Fig. 9(e), which indicates that there is in-plane exchange bias effect. We have also measured the ANE contribution in the

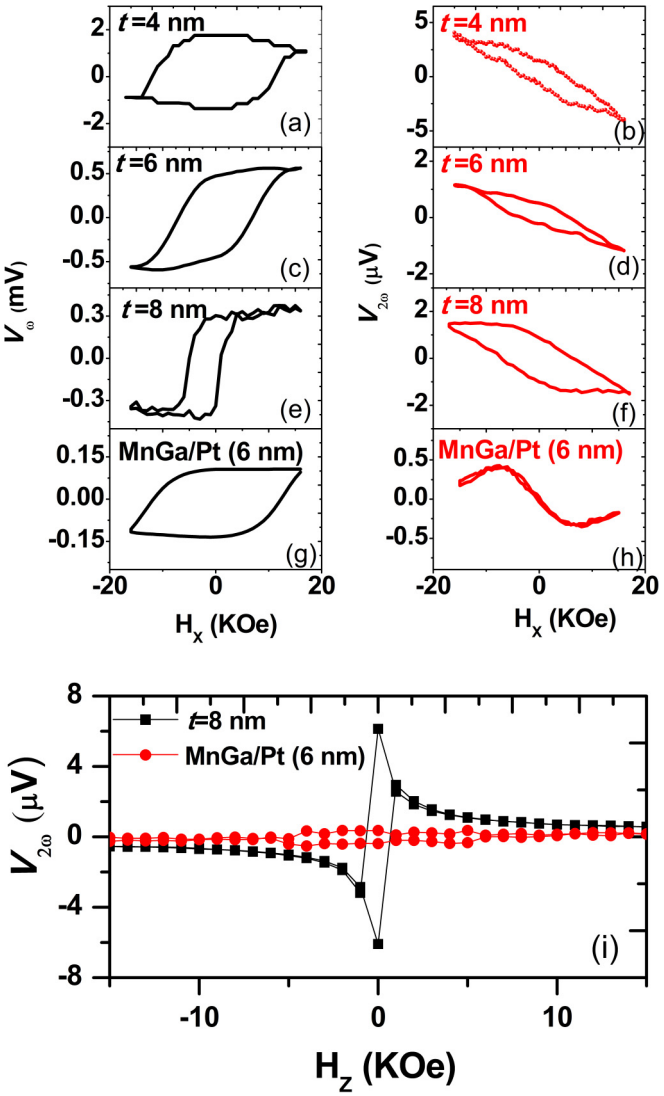

FIG. 9. (a)–(h) First V_ω and second $V_{2\omega}$ harmonic Hall voltages plotted against the H_X for all the four films. (i) Second $V_{2\omega}$ harmonic Hall voltages plotted against the H_Z for the $t = 8$ nm and MnGa/Pt (6 nm) films.

MnGa/IrMn (8 nm) and MnGa/Pt (6 nm) films with sweeping the magnetic field along the out-of-plane direction, as shown in Fig. 9(i). As discussed in Ref. [16], the differences in $V_{2\omega}$ at positive and negative saturated magnetic field in the two films are all very small, indicating small ANE. However, as the field sweeps to zero, there is a peak in $V_{2\omega}(H)$ for the $t = 8$ nm film corresponding to the second harmonic signal with $H = 0$ Oe in Fig. 7. We cannot confirm whether this signal stems from SOT, ANE, or the complex domain structure in the MnGa/IrMn films, and we hope that our results will motivate further theoretical and experimental efforts to uncover this complex mechanism of the SOT using IrMn.

IV. SUMMARY

In conclusion, we have systematically investigated the AHE and SOT in the MnGa/IrMn films, in which a single $L1_0$-MnGa epitaxial layer reveals obvious orbital 2CK effect. The strong

SHE of IrMn has suppressed the orbital 2CK effect and modified the AHE of MnGa. The results are compared with the MnGa/Al and MnGa/Pt films. A scaling involving multiple competing scattering mechanisms has been used to distinguish different contributions to the modified AHE. It is found that these two kinds of spin dependent transport properties in the MnGa/HM (IrMn or Pt) are quite different from those in the MnGa single layer and MnGa/Al films in which Al displays very weak SHE. On the other hand, the sizeable SOT in the MnGa/IrMn films induced by the strong SHE of IrMn has also been observed. The IrMn layer supplies an in-plane exchange bias field and enables nearly field-free magnetization reversal. By performing adiabatic harmonic Hall voltage measurements, we also quantitatively investigated the SHE induced effective field.

ACKNOWLEDGMENTS

This work was partially supported by the National Basic Research Program of China (Grant No. 2015CB921502) and the National Science Foundation of China (Grants No. 61404125, No. 51371024, No. 51325101, and No. 51271020).

[1] J. E. Hirsch, Phys. Rev. Lett. **83**, 1834 (1999).
[2] I. M. Miron, K. Garello, G. Gaudin, P. J. Zermatten, M. V. Costache, S. Auffret, S. Bandiera, B. Rodmacq, A. Schuhl, and P. Gambardella, Nature **476**, 189 (2011).
[3] L. Q. Liu, C.-F. Pai, Y. Li, H. W. Tseng, D. C. Ralph, and R. A. Buhrman, Science **336**, 555 (2012).
[4] K. Garello, I. M. Miron, C. O. Avci, F. Freimuth, Y. Mokrousov, S. Blügel, S. Auffret, O. Boulle, G. Gaudin, and P. Gambardella, Nat. Nanotechnol. **8**, 587 (2013).
[5] H. Nakayama, M. Althammer, Y.-T. Chen, K. Uchida, Y. Kajiwara, D. Kikuchi, T. Ohtani, S. Geprägs, M. Opel, S. Takahashi, R. Gross, G. E. W. Bauer, S. T. B. Goennenwein, and E. Saitoh, Phys. Rev. Lett. **110**, 206601 (2013).
[6] J. Kim, J. Sinha, M. Hayashi, M. Yamanouchi, S. Fukami, T. Suzuki, S. Mitani, and H. Ohno, Nat. Mater. **12**, 240 (2013).
[7] L. Q. Liu, O. J. Lee, T. J. Gudmundsen, D. C. Ralph, and R. A. Buhrman, Phys. Rev. Lett. **109**, 096602 (2012).
[8] S. Emori, U. Bauer, S.-M. Ahn, E. Martinez, and G. S. D. Beach, Nat. Mater. **12**, 611 (2013).
[9] K. K. Meng, J. Miao, X. G. Xu, J. X. Xiao, J. H. Zhao, and Y. Jiang, Phys. Rev. B **93**, 060406(R) (2016).
[10] C. O. Avci, K. Garello, C. Nistor, S. Godey, B. Ballesteros, A. Mugarza, A. Barla, M. Valvidares, E. Pellegrin, A. Ghosh, I. M. Miron, O. Boulle, S. Auffret, G. Gaudin, and P. Gambardella, Phys. Rev. B **89**, 214419 (2014).
[11] G. Yu, P. Upadhyaya, Y. Fan, J. G. Alzate, W. Jiang, K. L. Wong, S. Takei, S. A. Bender, L.-T. Chang, Y. Jiang, M. Lang, J. Tang, Y. Wang, Y. Tserkovnyak, P. K. Amiri, and K. L. Wang, Nat. Nanotechnol. **9**, 548 (2014).
[12] C. Zhang, S. Fukami, H. Sato, F. Matsukura, and H. Ohno, Appl. Phys. Lett. **107**, 012401 (2015).
[13] S. Fukami, C. L. Zhang, S. DuttaGupta, A. Kurenkov, and H. Ohno, Nat. Mater. **15**, 4 (2016).
[14] T. Suzuki, S. Fukami, N. Ishiwata, M. Yamanouchi, S. Ikeda, N. Kasai, and H. Ohno, Appl. Phys. Lett. **98**, 142505 (2011).
[15] X. Qiu, K. Narayanapillai, Y. Wu, P. Deorani, D.-H. Yang, W.-S. Noh, J.-H. Park, K.-J. Lee, H.-W. Lee, and H. Yang, Nat. Nanotechnol. **10**, 333 (2015).
[16] X. Qiu, P. Deorani, K. Narayanapillai, K.-S. Lee, K.-J. Lee, H.-W. Lee, and H. Yang, Sci. Rep. **4**, 4491 (2014).
[17] E. H. Hall, Philos. Mag. **10**, 301 (1880).
[18] A. Hoffmann, IEEE Trans. Magn. **49**, 5172 (2013).
[19] R. Karplus and J. M. Luttinger, Phys. Rev. **95**, 1154 (1954).
[20] G. Sundaram and Q. Niu, Phys. Rev. B **59**, 14915 (1999).
[21] T. Jungwirth, Q. Niu, and A. H. MacDonald, Phys. Rev. Lett. **88**, 207208 (2002).
[22] M. Onoda and N. Nagaosa, J. Phys. Soc. Jpn. **71**, 19 (2002).
[23] J. Sinova, D. Culcer, Q. Niu, N. A. Sinitsyn, T. Jungwirth, and A. H. MacDonald, Phys. Rev. Lett. **92**, 126603 (2004).
[24] D. Xiao, M.-C. Chang, and Q. Niu, Rev. Mod. Phys. **82**, 1959 (2010).
[25] J. Smit, Physica (Amsterdam) **21**, 877 (1955).
[26] L. Berger, Phys. Rev. B **2**, 4559 (1970).
[27] A. Crepieux and P. Bruno, Phys. Rev. B **64**, 014416 (2001).
[28] S. Onoda, N. Sugimoto, and N. Nagaosa, Phys. Rev. Lett. **97**, 126602 (2006).
[29] T. Miyasato, N. Abe, T. Fujii, A. Asamitsu, S. Onoda, Y. Onose, N. Nagaosa, and Y. Tokura, Phys. Rev. Lett. **99**, 086602 (2007).
[30] Y. Tian, L. Ye, and X. Jin, Phys. Rev. Lett. **103**, 087206 (2009).
[31] D. Z. Hou, G. Su, Y. Tian, X. F. Jin, S. Y. A. Yang, and Q. Niu, Phys. Rev. Lett. **114**, 217203 (2015).
[32] J. L. Xu, Y. F. Li, D. Z. Hou, L. Ye, and X. F. Jin, Appl. Phys. Lett. **102**, 162401 (2013).
[33] C. Zeng, Y. Yao, Q. Niu, and H. H. Weitering, Phys. Rev. Lett. **96**, 037204 (2006).
[34] L. J. Zhu, S. H. Nie, P. Xiong, P. Schlottmann, and J. H. Zhao, Nat. Commun. **7**, 10817 (2016).
[35] D. L. Cox and A. Zawadowki, Adv. Phys. **47**, 599 (1998).
[36] Y. -W. Oh, S. C. Baek, Y. M. Kim, H. Y. Lee, K.-D. Lee, C.-G. Yang, E.-S. Park, K.-S. Lee, K.-W. Kim, G. Go, J.-R. Jeong, B.-C. Min, H.-W. Lee, K.-J. Lee and B.-G. Park, Nat. Nanotechnol. **11**, 878 (2016).
[37] A. van den Brink, G. Vermijs, A. Solignac, J. Koo, J. T. Kohlhepp, H. J. M. Swagten, and B. Koopmans, Nat. Commun. **7**, 10854 (2016).
[38] L. J. Zhu, D. Pan, S. H. Nie, J. Lu, and J. H. Zhao, Appl. Phys. Lett. **102**, 132403 (2013).
[39] R. Mathieu, A. Asamitsu, H. Yamada, K. S. Takahashi, M. Kawasaki, Z. Fang, N. Nagaosa, and Y. Tokura, Phys. Rev. Lett. **93**, 016602 (2004).
[40] W. Zhang, M. B. Jungfleisch, W. Jiang, J. E. Pearson, A. Hoffmann, F. Freimuth, and Y. Mokrousov, Phys. Rev. Lett. **113**, 196602 (2014).
[41] W. Zhang, M. B. Jungfleisch, F. Freimuth, W. Jiang, J. Sklenar, J. E. Pearson, J. B. Ketterson, Y. Mokrousov, and A. Hoffmann, Phys. Rev. B **92**, 144405 (2015).
[42] R. Ramaswamy, X. Qiu, T. Dutta, S. D. Pollard, and H. Yang, Appl. Phys. Lett. **108**, 202406 (2016).
[43] C. O. Avci, K. Garello, M. Gabureac, A. Ghosh, A. Fuhrer, S. F. Alvarado, and P. Gambardella, Phys. Rev. B **90**, 224427 (2014).